

Preliminary Implementation of Geophysical Techniques to Monitor Embankment Dam Filter Cracking at the Laboratory Scale

Robert V. RINEHART¹, Minal L. PAREKH², Justin B. RITTGERS³, Michael A. MOONEY⁴,
and Andre REVIL⁵

¹Civil Engineer, Materials Engineering & Research Laboratory, Bureau of Reclamation
PO Box 25007, Denver, CO 80225; e-mail: rrinehart@usbr.gov

²Graduate Student, SmartGeo Program, Colorado School of Mines
1500 Illinois Street, Golden, CO 80401; e-mail: mparekh@mines.edu

³ Graduate Student, SmartGeo Program, Colorado School of Mines
1500 Illinois Street, Golden, CO 80401; e-mail: jrittger@mines.edu

⁴Professor, Civil & Environmental Engineering Department, Colorado School of Mines
1500 Illinois Street, Golden, CO 80401; e-mail: mooney@mines.edu

⁵ Professor, Geophysics Department, Colorado School of Mines
1500 Illinois Street, Golden, CO 80401; e-mail: arevil@mines.edu

Internal erosion presents a significant hazard to water retaining structures and is most often identified in its progressive stages through visual inspections or observations. Acoustic or ultrasonic methods in combination with electrical geophysical methods can be used as a tool for detection and continuous monitoring of subsurface internal erosion initiation in its early stages. This research investigates passive acoustic emission, self potential, and cross-hole tomography for suitability as long-term, remote and continuous monitoring techniques for internal erosion and cracking of embankment dams. Geophysical data from the three techniques have been collected during manually imposed cracking of granular filter materials. Specifically, data has been collected during both self-healing (i.e., desirable filter behavior) and during continuing erosion (i.e., undesirable filter behavior). The data is compared to baseline, pre-crack data. This proof-of-concept research provides evidence of these geophysical techniques for effective monitoring of embankment cracking as a precursor to internal erosion. This paper presents the details of the instrumentation systems, data acquisition parameters, and early findings from the research. 2D seismic velocity tomograms, passive acoustic and passive electrical signatures associated with cracking and suffusion are discussed.

Key Words

geophysics, cross hole tomography, self potential, passive acoustic emission, internal erosion, embankment dam filters, continuous remote monitoring

I INTRODUCTION

Internal erosion in earthen embankments (dams, levees) occurs when a critical combination of hydraulic gradient, in-situ stress conditions, soil porosity and intrinsic permeability, and material properties results in increased and uncontrolled seepage. This leads to the transport and migration of soil particles in a localized area, often at a crack in the soil (e.g., from desiccation, settlement, or seismic activity). Internal erosion presents a significant hazard to embankment dams, dikes, levees, abutments, spillways, and foundations, and a review of historical dam failures shows that about half of all embankment dam failures are related to internal erosion [Foster, 1998; Schmertmann, 2000]. This critical failure mode is difficult to detect in early stages, and typically is not identified until it has progressed to a full piping situation [Foster, 2008]. Further, a broad search of the literature indicates that acceptable means of determining the factor of safety against internal erosion have not been determined. It is also recognized that it is dangerous to place undue

¹ Corresponding author

confidence in a structure based on years of successful performance as internal erosion incidents can manifest after decades of satisfactory performance – underscoring the need for continuous monitoring.

Signs of active internal erosion, including sink holes, sand boils, and muddy seepage, are often discovered by local residents or during periodic visual safety inspections. Alternatively, identifying the onset and progression of internal erosion by continuously and remotely monitoring for subsurface changes would be preferred, allowing for early intervention and risk reduction. Several geophysical techniques are believed to hold potential as monitoring tools, including passive Acoustic Emission (AE), Self Potential (SP), and cross-hole direct-transmission sonic tomography (CT) are further discussed below.

Internal erosion can be mitigated by incorporating granular filter zones into the embankment, to filter or retain embankment soils and prevent particle migration. The Bureau of Reclamation, in partnership with the U.S. Army Corps of Engineers has been conducting large scale embankment filter research for several years to gain a better understanding of: cracked filter performance, conditions which cause a crack within a filter, ability of a filter to heal under flow conditions, and effectiveness of a filter to stop or control flow [Redlinger, 2012]. A laboratory model referred to as the soil crack box was constructed (Figure 1). The box allows for the compaction of filter material in various configurations, subsequent cracking of the filter (i.e., to simulate differential settlement, desiccation, or seismically induced cracking), and impingement of reservoir water upon the cracked filter.

The present work includes SP electrodes installed near the surface of the granular filter within the crack box, CT logging tubes (one transmitter, one receiver) installed through the full height of the filter on both sides of the crack zone, and AE monitoring using periodic passive recording from the CT receivers (geophones). Data have been collected via the three methods before filter cracking, during cracking, and during active water flow through the cracked filter. This paper presents the test set-up, geophysical instrumentation, and promising preliminary results.

II LABORATORY SETUP

II.1 Laboratory Embankment Filter Model

The geometry of the laboratory filter model (soil crack box) simulates field geometric conditions, and performs similarly to a granular embankment dam filter. The observed seepage is constant head, and the induced cracks are similar to those that occur in earthen embankments. The resulting design, shown in Figure 1, includes several components: a 2000 liter reservoir large enough to provide near-constant water supply, a 7 m³ zone to contain embankment and filter materials, and a 2.75 m long channel through which water passes from the reservoir to the embankment material. The box is constructed in two identical halves and hinged at the bottom centerline. Once full of material (Figure 1d), hydraulic jacks force the box to pivot at the hinge, inducing a crack (2.5 cm, typical) within the material (Figure 1e). The size of the box allows placement and compaction using vibratory methods similar to those used in the field. Potential seepage paths through the apparatus (i.e. hinges, joints) were thoroughly sealed with silicone caulk to minimize leaking. Sandpaper was installed along the walls confining the filter material to provide friction intended to simulate shear resistance provided by confinement. A drain was installed on each side of the floor of the material box to allow drainage below the filter material (simulating a drain below a filter zone). Drainage can be measured through outlet pipes. The drains can also be closed to

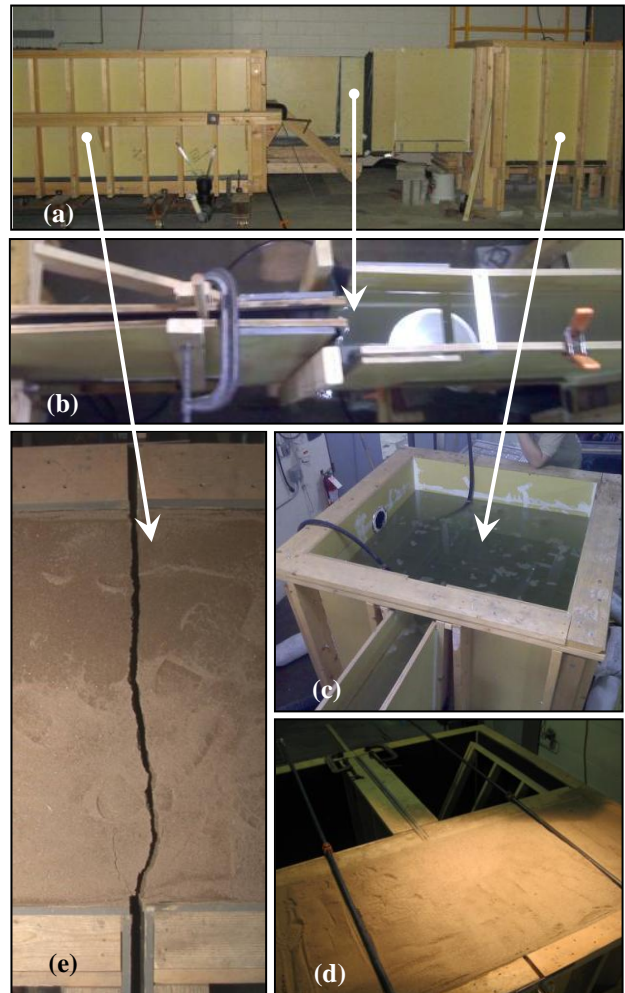


Figure 1: Laboratory layout of filter model showing: (a) assembled model, (b) upstream channel, (c) constant head reservoir, (d) uncracked filter, and (e) cracked filter (2.5 cm)

prevent drainage (simulating a filter that is isolated, or a drain that is clogged).

During a typical test the reservoir is released by removing a solid gate between the upstream channel and the reservoir. Water flows into and through the filter material in the box. Filter performance is observed and judged qualitatively by the material’s ability to sustain a crack, heal a crack under flow conditions, and stop or control flow through cracks. For more detail please refer to [Redlinger, 2012].

II.2 Geophysical Techniques

One means to continuously monitor for concentrated seepage and internal erosion is passive Acoustic Emission (AE) monitoring. AE monitoring involves using acoustic transducers (e.g., geophones or accelerometers) to passively “listen” for acoustic energy that is released from internal sources including earthquakes, impact or gradual loading forces, and impulsive sources (e.g., collapse events). Research regarding AE in soils has been ongoing since the 1970s [Koerner, 1976, 1981; Buck, 1986; Hung, 2009] and recent work by the United States Department of Agriculture and Ole Miss University has shown that AE exists due to internal erosion [Lu, 2004; Hickey, 2010]. In cases where data from several seismic monitoring stations are available, AE source localization can be performed through triangulation or a variety of more complex techniques. Research has shown that sudden or gradual increases in the rate or magnitude of AE events can be linked to cracking or internal erosion [Talwani, 1984, 1997].

A second potential means to continuously monitor for internal erosion is through the implementation of compressional seismic wave (p-wave) or shear wave (s-wave) cross-hole tomography (CT). Similar to AE monitoring, this technique utilizes acoustic transducers, only in the case of CT, recorded energy is from ‘active’ or intentionally generated vibrational or impact-type sources. The transmitters and receivers are accurately time-synchronized, and similar to CAT scan medical imaging technology, CT is performed using a multitude of transmitter-receiver pair geometries, helping to illuminate the materials between borehole pairs (e.g., see Figure 2). This geophysical technique allows for reconstruction of the spatial distribution of seismic velocity, related to the material’s density and elastic properties including the bulk and shear moduli. By repeating the data acquisition over time, this imaging could prove useful in tracking the evolution of subsurface features (i.e., time-lapse geophysics).

A third promising means to continuously monitor for internal erosion and concentrated seepage is through the use of the Self Potential (SP) method. The SP technique involves the measurement of the variation of the electrical potential distributions across the ground surface (or within boreholes) with respect to both space and time. These electrical potentials are associated with very small subsurface electric fields created by a variety of sources, including fluid flow through porous media (i.e., streaming potential). SP can help to quickly map the lateral location and geometry of preferential flow paths in the X-Y plane [Crespy, 2008]. The addition of other information about the electrical conductivity and material properties allows for the SP data to be inversely modeled to retrieve more useful quantitative parameters such as depth to the phreatic surface and groundwater flow velocity distributions [Sheffer, 2007]. Inverse analysis of SP data may prove useful, in that 3D fluid flow velocity distributions can be solved for within the first order, offering information on the severity and geometry of open transverse cracks, internal erosion and related concentrated seepage pathways within earth embankment structures.

II.3 Instrumented Tests

Geophysical instrumentation was included in two filter experiments: a two stage filter comprised of poorly graded sand upstream of poorly graded gravel (designated T11, Figure 3), and a single stage filter comprised of poorly graded sand (designated T12, Figure 4). The sand material met the requirements (including gradation) for fine aggregate in ASTM C33. Generally, C33 fine aggregate (commonly referred to as concrete sand) is considered a good all-purpose filter material, capable of filtering a wide

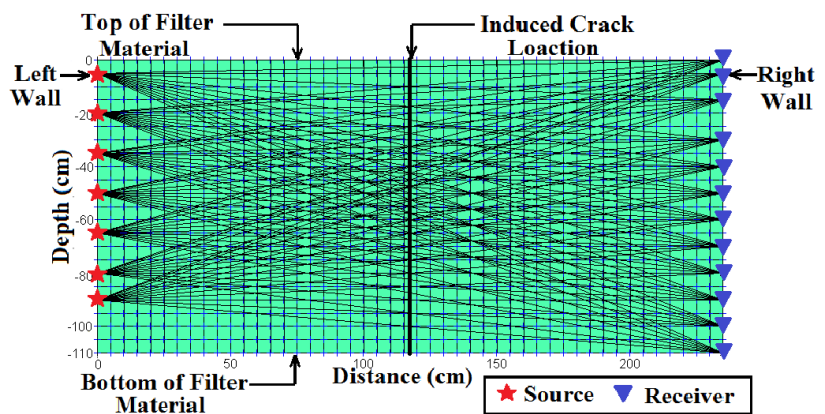


Figure 2. Approximate CT raypath coverage between source (left edge) and receiver (right edge) locations for T11 and T12 (boxes represent discretization for tomography modeling)

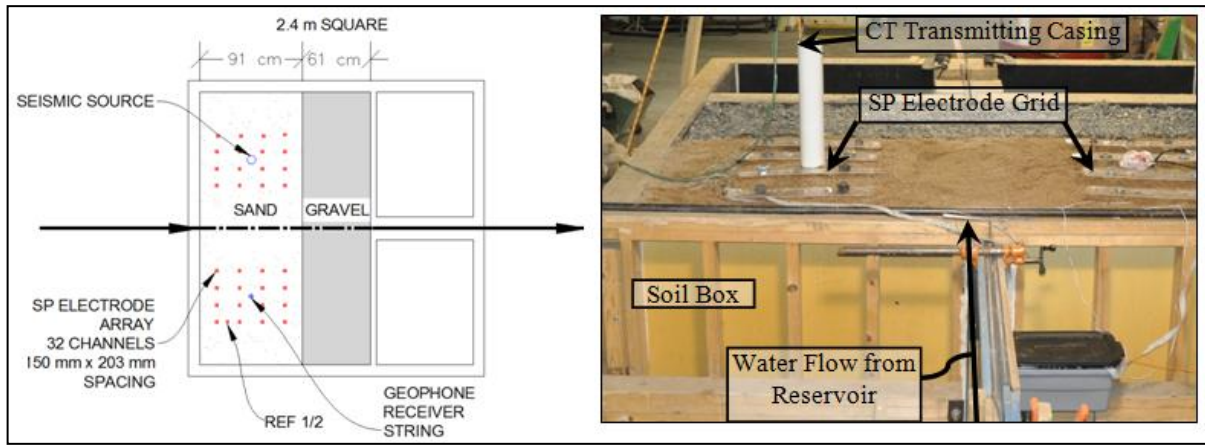


Figure 3. Schematic (left) and pre-crack photograph (right) of filter geometry and instrumentation for T11 – two stage filter

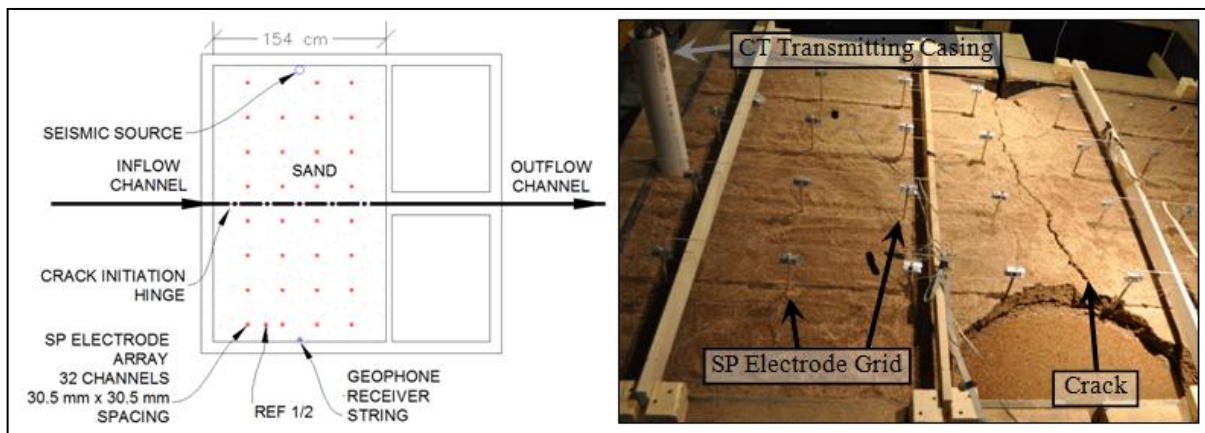


Figure 4. Schematic (left) and post-crack photograph (right) of filter geometry and instrumentation for T12 – single stage filter

range of embankment materials. The gradation of the gravel, which had a maximum particle size of 19 mm, was filter-compatible with the gradation of the sand. Both the sand and gravel materials contained less than 2% fines at the time of compaction.

Filter materials were compacted in the box using a vibratory plate. In-situ moisture and density were determined using the sand cone test (ASTM D1556). Average dry unit weights for the sand material were 16.9 kN/m^3 and 17.4 kN/m^3 for tests T11 and T12, respectively. Moisture content for the sand material was 5.0% for both tests. The gravel material was not tested, but received the same compactive effort (i.e., number of passes with the vibratory plate) as the sand.

Figures 3 and 4 show schematics and photographs of the geophysical instrument layout for tests T11 and T12, respectively. For both tests, SP electrodes were placed in contact with the surface of the poorly graded sand material on a grid spacing within the crack box. A harness, configured to minimize impact to the crack zone, prohibited electrode movement. For T11, electrodes were mounted to the underside of acrylic sheeting with the electrode grids offset 38 cm from the crack alignment. For T12, electrodes were mounted to rods suspended from a frame located approximately 15 cm above the soil surface to allow the electrodes to be in firm contact with the soil, but to also allow the soil to move freely beneath them. SP data were collected on 32 channels using a BioSemi EEG multi-channel, high resolution electrical potential measurement system. Specifications for geophysical applications using a BioSemi system can be found in [Crespy, 2008]. Electrical potentials were measured with respect to a reference electrode (“REF1/2” on Figures 3 and 4).

Casings for CT transmitting and receiving (76 mm inside diameter PVC pipe) were installed through the full height of the sand, offset 1.2 m from the crack alignment on both sides for T11 (Figure 3) and placed along the inside wall of the box for T12 (Figure 4). The seismic source, an Olson Instruments P-SV triaxial impact source triggered through Olson’s Freedom Data PC system, is a down-hole source capable of

generating shear and compressional waves by directly impacting the inside of the casing at a set depth. For these tests, the source depth ranged from 5 cm to 90 cm below the surface, generally at 15 cm intervals (Figure 2). The receiver array was comprised of twelve 10 Hz center-frequency geophone transducers and was also used to collect passive AE data. A Geometrics Geode seismic recorder acquired signals from the geophone receiver string. Tomographic data waveforms were acquired using a sample interval of 0.25 ms over a duration of 0.20 s to 0.25 s. The Geode also acquired AE waveforms at sample intervals of 0.20 to 0.25 ms over a 4 to 30 s duration.

The study included collecting data via the three geophysical methods before filter cracking (i.e., after compaction), during and after cracking, and while the crack in the filter material was subjected to focused water flow. For test T11, a 2.5 cm wide crack was opened and subjected to focused water flow with the drains in the bottom of the box open. The crack healed and did not result in flow to the downstream collection reservoir. The 2.5 cm wide crack was subjected to flow overnight without erosion or flow to the downstream collection reservoir. The following morning, the crack was opened to approximately 15 cm. The crack healed and did not result in flow to the downstream collection reservoir.

For test T12, a 2.5 cm wide crack was opened and subjected to focused water flow, with the drains in the bottom of the box open. The crack healed and did not result in flow to the downstream collection reservoir. The 2.5 cm crack was subjected to flow overnight without erosion or flow to the downstream collection reservoir. The following morning, the drains in the bottom of the box were closed and the crack was again subjected to water overnight. The crack healed and did not result in flow to the downstream collection reservoir. The following day, the crack was opened incrementally (approximately 1.25 cm/6 min) to approximately 15 cm with the drains closed. The crack collapsed and healed several times, until the filter failed and allowed uncontrolled flow to continue to the downstream collection reservoir.

Digital video cameras positioned at the upstream reservoir, two angles downstream of the filter material, and directly overhead of the crack captured video during the cracking and flow events and provided a visual reference for the timing of erosion and healing events.

III PRELIMINARY RESULTS

III.1 Passive Acoustic Emission

AE data were recorded for several hours and on various days throughout each test using repeated 4, 10 or 30 s records. The recorded frequencies ranged from approximately 5 to 250 Hz, which allowed for identification of unique spectral signatures at various stages of internal erosion, overtopping flow, collapse events and self-healing phenomena that occurred throughout the filter tests. Preliminary results of this portion of the study are shown in the spectrograms presented in Figure 5. Here, the power spectrums of AE data are plotted as a function of time for three representative, 30-second time periods. The color scale of the three panels represents normalized power at a given frequency and record time (power spectra averaged for each second of recorded data). Warmer colors (i.e., reds and yellows) represent higher energy levels and more activity, while cooler colors (i.e., blues and greens) represent lower energy levels and less activity at a given frequency. Within the recorded spectra, bands of high power noise at relatively low-frequencies (e.g., 10-50 Hz) associated with the laboratory utility duct-work and nearby machinery dominate the signal. Electrical power-grid noise is also apparent in the data as high-energy bands (red) at 60 Hz and its harmonics (120 Hz and 180 Hz).

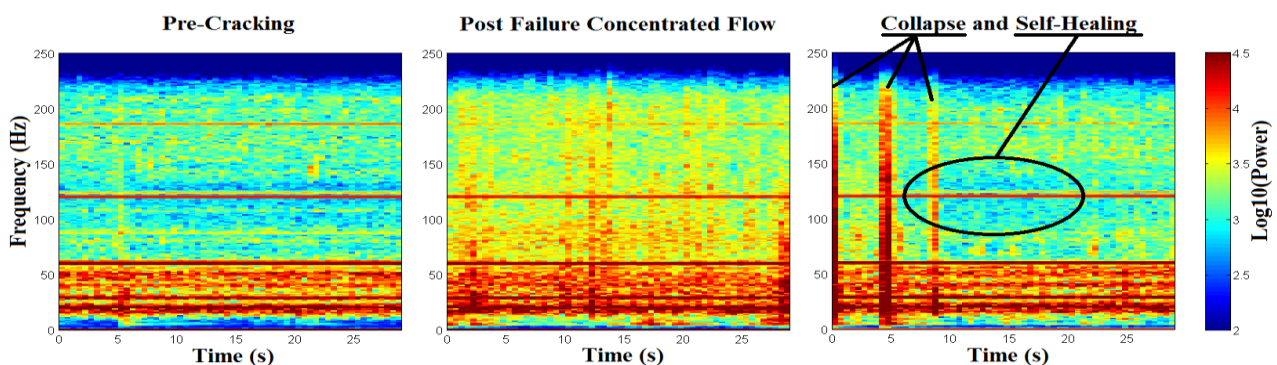


Figure 5. AE signatures during three stages of T12: Pre-cracking baseline (left), post filter cracking during concentrated flow (center), and subsequent sidewall-collapse and self-healing events (right)

Comparison of the pre-cracking baseline data and data collected during concentrated flow (left and center panels of Figure 5, respectively) shows a spectral distinction between the two stages of the test. The right-hand panel of Figure 5 shows broad-band events representing a collapse event, where the sidewalls of the induced crack collapsed into the open fracture. The relatively high energy observed at higher frequencies during concentrated flow (center panel) disappears after the collapse events, indicating cessation concentrated flow due to self-healing of the filter material. These preliminary results show important and noticeable relationships between AE signatures and erosion phenomena. As seen in Figure 5, unique AE signatures of filter collapse and self-healing were observed during these experiments, showing promise for the successful use of the AE method in monitoring applications for full-scale embankment structures.

III.2 Cross-hole Tomography

Preliminary results of the cross-hole p-wave tomography data are presented in Figures 6 and 7. Figure 6 shows the change in p-wave arrival time with travel distance between source-receiver pairs (note that an increase in arrival time with similar offset indicates lower velocity). The data contain trends that suggest an overall decrease in p-wave velocities with cracking, relative to the pre-crack data set from T12. The progressive slowing of the material velocity likely reflects a decrease in the stress field due to the cracking, increase in water content, and/or loosening of the compacted filter materials.

Figure 7 depicts velocity tomograms calculated for each time step during T12 (pre-crack, 2hrs and 24hrs after cracking and initiation of flow). CT data acquisition was achieved by integrating two separate seismic systems: one system generated the seismic source, and the other system recorded the data at the receivers. Interfacing these two systems resulted in a timing mismatch between the source (time-zero) and the beginning of each seismic CT record, and while the absolute time synchronization discrepancy is unknown, it was consistent for all data recorded. As a result, all calculated velocities presented here are considered relative and not absolute seismic velocities. Velocities presented in the tomograms shown on Figure 7 are slower than expected true velocities of the filter material, however the relative changes between time steps represent true or absolute decreases in p-wave velocity.

A progressive overall decrease in the p-wave velocity distribution can be seen in each subsequent tomogram moving left to right in Figure 7. More noticeable changes occur between the two and 24-hour tomograms than between the zero and two hour tomograms. This may be due to the infiltration of moisture into the materials surrounding the crack and throughout the filter material, helping to homogenize the velocity distribution within the filter model. Still, a noticeable decrease in velocity is captured using the tomography

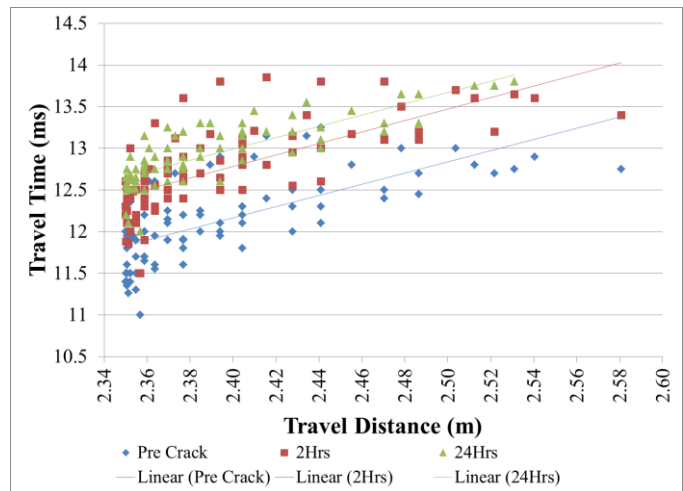


Figure 6. Scatter plots of p-wave travel time versus source-receiver separation for T12 data. Trend lines have been added to depict the overall relative decrease in calculated velocities over the course of T12.

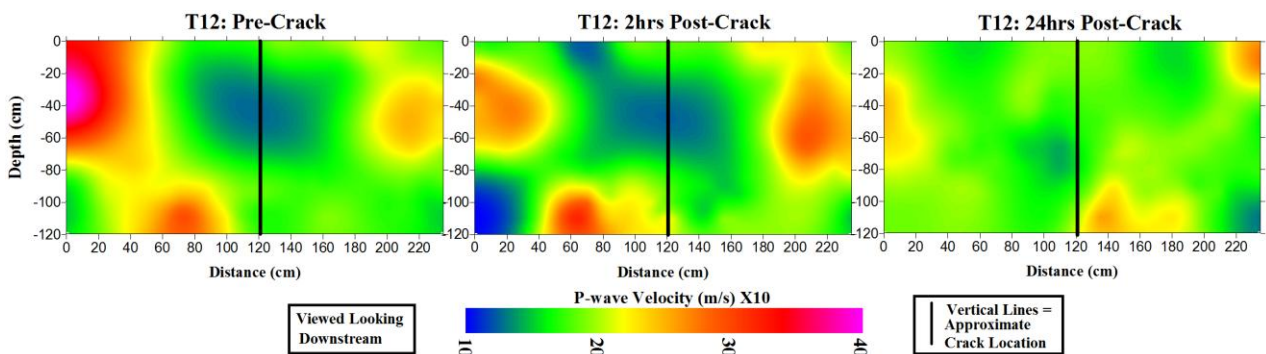


Figure 7. P-wave tomograms for T12 data collected pre-crack (left panel), and 2hrs and 24hrs after cracking of filter material and subjection to concentrated flow (center panel and right panel respectively)

method. Unfortunately, failure of the filter material happened too quickly after collecting the 24hr post-crack data set, preventing collection of post-failure data sets. We expect that further internal erosion and sloughing of materials leading up to and during the failure events of T12 would have further decreased the stress field and hence the p-wave velocities within the filter materials. These results show promise for the applicability of seismic tomography techniques for successfully detection and imaging of filter material cracking and failure phenomena within earthen embankment structures.

III.3 Self Potential

Preliminary SP results are shown in Figure 8, where contour plots of SP data are presented for select times during T11. Figure 8 depicts a sequence of snapshots of the electrical potential distribution across the top surface of the filter material (plan view) where the SP electrodes were installed. These contour images depict the development of a positive SP anomaly typically associated with the flow of fluid through porous media. Here, water is flowing from right to left, and the resultant SP anomaly is seen to develop in a progressive fashion in the downstream direction. The SP anomaly is located above the majority of concentrated fluid flow within the filter material, near the crack alignment. The physical mechanism that causes the SP anomaly seen in Figure 8 is proportional to the velocity of fluid flow through the filter material. Therefore, the observed SP anomaly is expected to develop in the vicinity of concentrated flow through the filter material, and is expected to subside in the advent of self-healing phenomena that decrease or stop flow entirely. This observed and expected relationship between SP data and the state of the filter material offers promise in the applicability of the SP technique towards full-scale embankment time-lapse monitoring efforts.

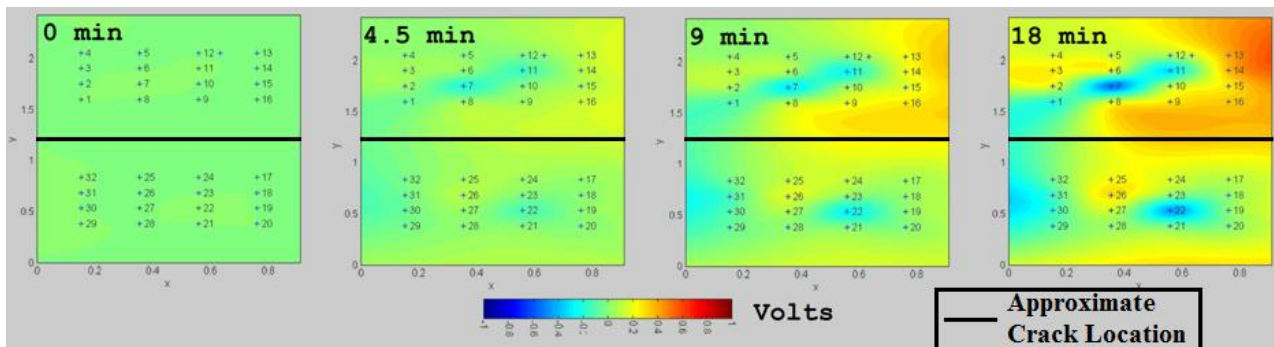


Figure 8. Plan view contour plots of electric potential distributions (SP data) at select time-steps after initial cracking of filter material and subsection to fluid flow during T11.

IV CONCLUSIONS AND APPLICATIONS

The threat of embankment failure from uncontrolled flow through a crack is exacerbated not only by the lack of understanding of the parameters contributing to cracking, healing, and flow control, but also by the absence of early detection and monitoring methods capable of identifying the process in its early stages. Applications using time-lapse geophysics hold promise for detecting spatial and temporal changes in the subsurface conditions through continuous monitoring. This paper describes some promising signatures in geophysical signals associated with cracking, concentrated flow, and collapsing and healing. While the laboratory is a controlled environment, a large amount of man-made ambient noise exists with respect to seismic and electrical signals. Despite this challenging data acquisition environment, we have demonstrated that precursory internal erosion phenomena, collapse and subsequent healing events are evident and well above the spectral noise floors of the SP and AE data presented herein. CT-measured changes in the seismic velocity distributions as a result of crack formation, concentrated flow and fluid infiltration are quite evident. The time lapse SP signatures clearly indicate water flowing through the partially saturated soil concentrated along the induced crack.

These various patterns can be used to develop data analysis algorithms for automated detection of cracking and self-healing events, and early notification of these potential risks within earthen embankment structures. A time-lapse monitoring system can be used to describe baseline signals and to set thresholds for notification. Work remains to further understand the link between identifiable cracking, healing, and flow events, as well as the risk of filter failure, in order to provide a complete picture for dam safety decision making. Our research in the cracked filter box is ongoing; however, this study serves as a preliminary proof

of concept. For a full scale earth dam, direct application in the form of buried geophones, surface geophones or other types of seismic transducers and/or surface SP electrodes can augment conventional instrumentation to enable a higher resolution (in time and in space) response that might otherwise go unnoticed by traditional instrumentation and visual methods.

V ACKNOWLEDGEMENTS

The authors are grateful for financial assistance provided by the Bureau of Reclamation Science & Technology Program, U.S. Army Corps of Engineers Risk Management Center, National Science Foundation (NSF IGERT Program: DGE-0801692), and the Hydroresearch Foundation. The authors are indebted to Olson Engineering, Inc. for the generous loan of their cross-hole tomography equipment.

VI REFERENCES

Buck, C. J., and Watters, R. J., (1986). “Acoustic Emission Generation From Water Flow Through Granular Soils.” In *Proceedings of the 22nd Symposium on Engineering Geology and Soils Engineering*, 138–154. Boise, Idaho.

Crespy, A., Revil, A., Linde, N., Byrdina, S., Jardani, A., Bolève, A., and Henry, P., (2008), Detection and localization of hydromechanical disturbances in a sandbox using the self-potential method, *Journal of Geophysical Research*, 113, B01205, doi: 10.1029/2007JB005042.

Foster, M., Fell, R., Vroman, N., Cyganiewicz, J., Sills, G., and Davidson, R., (2008). “Seepage and Piping Toolbox--Continuation, Progression, Intervention, and Breach.” In *28th Annual United States Society on Dams Conference: The Sustainability of Experience--Investing in the Human Factor*, 1049–1064. Portland, Oregon.

Foster, M.A., Fell, R., and Spannagle, M. (1998). Analysis of Embankment Dam Incidents, *UNICIV Report No. R-374*, University of New South Wales, Sydney, Australia.

Hickey, C., Ekimov, A., Hanson, G., and Sabatier, J., (2010). “Time-Lapse Seismic Measurements on a Small Earthen Embankment During an Internal Erosion Experiment.” In *SAGEEP 2009 Proceedings*. Keystone, Colorado.

Hung, M-H., Lauchle, G. C., and Wang, M C., (2009). “Seepage-Induced Acoustic Emission in Granular Soils.” *Journal of Geotechnical and Geoenvironmental Engineering ASCE*, Vol. 135, No. 4, pp. 566–572.

Koerner, R. M., Lord, A. E., McCabe, W. M., and Curran, J. W., (1976). “Acoustic Emission Behavior of Granular Soils.” *Journal of the Geotechnical Engineering Division, ASCE* Vol. 102, No. GT7, pp 761–773.

Koerner, R. M., McCabe, W. M., and Lord, A. E., (1981). “Acoustic Emission Behavior and Monitoring of Soils.” In *Acoustic Emissions in Geotechnical Engineering Practice, A Symposium Sponsored by ASTM Committee D-18 on Soil and Rock for Engineering Purposes*, ed. V. P. Drnevich and R. E. Gray, pp 93–141. ASTM Publication Code Number 04-750000-38. Baltimore, MD: American Society for Testing and Materials.

Lu, Z., Hickey, C., and Sabatier, J., (2004). “Effects of Compaction on the Acoustic Velocity in Soils.” *Soil Science Society of America Journal* 68 (February): pp 7–16.

Redlinger, C., Rudkin, C., Hanneman, D., and Engemoen, W. (2012). “Lessons Learned from Large-Scale Filter Testing,” Manuscript Submitted March 2012 to 6th International Conference on Scour and Erosion, Paris, France, August 27-31, 2012.

Schmertmann, J. H. (2000). “The No-Filter Factor of Safety against Piping Through Sands,” *Geotechnical Special Publication No. 11 Judgement and Innovation, The Heritage and Future of the Geotechnical Engineering Profession*, pp. 65-132.

Sheffer, M., (2007), Forward modeling and inversion of streaming potential for the interpretation of hydraulic conditions from self-potential data, 2007 *Ph.D. Thesis, The university of British Columbia*, pp 6-8.

Talwani, P., (1997). “Seismotectonics of Koyna-Warna Region.” *Pure Applied Geophysics*.

Talwani, P., (1984). “Pore Pressure Diffusion and the Mechanism of Reservoir-Induced Seismicity.” *Pure Applied Geophysics*, 122: pp 122,947-965.